Field effect transistors and photodetectors based on nanocrystalline graphene derived from electron beam induced carbonaceous patterns

2012 Nanotechnology 23 425301

(http://iopscience.iop.org/0957-4484/23/42/425301)

Nanotechnology **23** (2012) 425301 (8pp) doi:10.1088/0957-4484/23/42/425301

Field effect transistors and photodetectors based on nanocrystalline graphene derived from electron beam induced carbonaceous patterns

Narendra Kurra, Venkata Srinu Bhadram, Chandrabhas Narayana and G U Kulkarni

Chemistry and Physics of Materials Unit and DST Unit on Nanoscience, Jawaharlal Nehru Centre for Advanced Scientific Research, Jakkur PO, Bangalore 560064, India

E-mail: kulkarni@jncasr.ac.in

Received 10 July 2012, in final form 25 August 2012
Published 4 October 2012
Online at stacks.iop.org/Nano/23/425301

Abstract
We describe a transfer-free method for the fabrication of nanocrystalline graphene (nc-graphene) on SiO_2 substrates directly from patterned carbonaceous deposits. The deposits were produced from the residual hydrocarbons present in the vacuum chamber without any external source by using an electron beam induced carbonaceous deposition (EBICD) process. Thermal treatment under vacuum conditions in the presence of Ni catalyst transformed the EBIC deposit into nc-graphene patterns, confirmed using Raman and TEM analysis. The nc-graphene patterns have been employed as an active p-type channel material in a field effect transistor (FET) which showed a hole mobility of $\sim$90 cm^2 V^{-1} s^{-1}. The nc-graphene also proved to be suitable material for IR detection.

S Online supplementary data available from stacks.iop.org/Nano/23/425301/mmedia

(Some figures may appear in colour only in the online journal)

1. Introduction

Graphite and diamond, the well-known allotropes of carbon, exhibit diverse physical and electrical properties due to different bonding, namely a prevalence of sp^2 or sp^3 hybridizations [1, 2]. A blend of the two hybridizations together with different morphological schemes leads to nanoallotropes of carbon with various dimensionalities—zero-dimensional fullerenes, one-dimensional carbon nanotubes and two-dimensional graphene [3, 4]. Among the nanoallotropes, graphene and its derivatives have become popular materials in recent years due to their extraordinary electrical, optical and mechanical properties [4–7].

There have been several methods for producing graphene, including micro-mechanical cleavage from graphite bulk crystals [4, 6], chemical exfoliation [5, 8], liquid-phase exfoliation [9] and chemical vapor deposition (CVD) over catalytic metal substrates [10]. However, a recent trend was to convert insulating carbon sources into conducting graphene through thermal treatment under suitable conditions. Thus, Tour and co-workers have demonstrated the growth of high quality graphene on Cu foils starting from natural carbon sources, such as food, insects and waste, by thermal treatment in forming gas [11]. It has been shown that the encapsulation of polymer films (such as polydimethylsiloxane (PDMS), poly(methyl methacrylate) (PMMA), and polystyrene) and self-assembled monolayers with Ni film (as a capping layer) followed by annealing leads to precipitation of bi- and tri-layer graphene directly on the chosen substrates [12–15]. Various other carbon sources such as amorphous and diamond-like carbon films have also been transformed into graphene by thermal treatment in the presence of metal catalyst [16–18]. CVD techniques without any catalyst have also been employed for direct

growth of graphene on insulating substrates [19–22]. Many such processes result in the formation of small graphene domains also termed nanocrystalline graphene (nc-graphene), whose properties have hardly been explored. Nevertheless, nc-graphene domains with interconnected networks have been projected for the applications in photovoltaics, transparent conducting electrodes and sensors [19–22].

In order to realize practical electronic devices, it is highly desirable to have graphene with a predefined shape and size at desired locations on dielectric substrates. In some instances, the prepared graphene flakes/ribbons on a substrate have been transferred to the desired substrate for device integration using PDMS as the transferring agent [23]. But most of the processes reported in the literature produce graphene sheets distributed randomly on a substrate, and locating them for device fabrication is usually tedious. It is therefore necessary to grow graphene directly on insulating SiO_2 substrates for ease of device fabrication.

Here we report a direct write method to obtain patterns of nc-graphene by vacuum annealing of electron beam induced carbonaceous (EBIC) deposits in the presence of Ni catalyst. Electron beam induced carbonaceous deposition (EBICD) is usually performed using hydrocarbon sources in the form of pump oil [24] and paraffin [25] or residual hydrocarbons [26] present in the vacuum environment of a scanning electron microscope (SEM). The hydrocarbon species produce carbonaceous deposits on a substrate under a focused electron beam. Since EBIC deposits are chemically robust and electrically insulating they have been employed as an etch resist for micromachining [27] and as a local dielectric in diode fabrication and CNT circuits [24, 26]. EBIC deposits have also been employed as a glue to lower the electrical contact resistance and strengthen the mechanical characteristics of CNT–metal electrode junctions [28] and CNT–atomic force microscope (AFM) tip interfaces [29]. In this study we describe selective growth of patterns of nc-graphene derived from insulating EBIC deposits and employ the obtained patterns to fabricate field effect transistors and infrared photodetectors.

2. Experimental details

SiO_2 (300 nm)/Si substrates were cleaned by sonicating in acetone and isopropanol followed by a rinse in double distilled water for 2 min. EBICD was performed using a field emission SEM (Nova Nano SEM 600, FEI Company) with a chamber pressure of 10^{-4} Torr, at a working distance of 3–4 mm. Selected regions on the substrate were exposed to electron dosages of 0.7–2.5 C cm^{-2} at 10 kV in the patterning mode [26]. Electron dosage increases with increasing time of exposure and number of passes. Electron dosage is a time dependent quantity and its formula is given by

$$\text{Area dosage} = (\text{beam current} \times \text{dwell time} \times \times \text{number of passes})/\text{area per pixel}.$$

The substrate deposited by EBICD was transferred to a physical vapor deposition (PVD) system and a Ni catalyst layer (thickness 10–40 nm) was deposited onto the EBICD surface at chamber pressure of 6×10^{-6} Torr. Vacuum annealing at 2×10^{-5} Torr was carried out in the PVD chamber at different temperatures (600–1100 °C) for 5–15 min. The steps involved in the fabrication of nc-graphene patterns from the EBIC deposits are shown in figure 1(a). EBIC deposits and nc-graphene patterns on a SiO_2/Si substrate were examined under an optical microscope (Laben, India). Raman spectra were recorded at different stages in the backscattering geometry using a 532 nm excitation from a diode pumped frequency doubled Nd:YAG solid state laser (model GDLM–5015L, Photop Swutech, China) and a custom-built Raman spectrometer equipped with a SPEX TRIAX 550 monochromator and a liquid nitrogen cooled CCD detector (Spectrum One with CCD3000 controller, ISA Jobin Yvon) [30]. AFM imaging was done on a diInnova scanning probe microscope (Veeco, USA) using Si probes (model RTESPA, spring constant 40 N m^{-1}) in tapping mode. Transmission electron microscopy (TEM) and selected area electron diffraction (SAED) analysis were performed using a JEOL-3010 instrument operating at 300 kV. For this purpose, vacuum annealed EBIC deposits on the SiO_2/Si surface were transferred to holey carbon film of the Cu TEM grid by lifting with a PMMA layer. Fifty microliters of 3 wt% PMMA ($M_w \sim 996$ kDa, Sigma-Aldrich) was drop-coated on the annealed EBIC patterns followed by curing at 180 °C for 5 min. The underlying SiO_2 was etched away using buffer oxide etchant (6:1 40% NH_4F and 49% HF) overnight and the floating PMMA films carrying nc-graphene were thoroughly washed in water. The support PMMA film was placed on the TEM grid and then dissolved away in acetone to leave behind nc-graphene on the grid which was subsequently dried [14].

A 60 nm thick Au film was deposited on the SiO_2/Si substrate by PVD (Hind Hivac, Bangalore) while using a carbon fiber (diameter, 6 μm) as a shadow mask which defined the source–drain electrodes (top contacts) for nc-graphene stripes. A Keithley-4200 semiconductor characterization system was used for measuring the device characteristics. All the measurements were carried out in ambient conditions. For photo-response measurements, a Nd:YAG laser with a wavelength of 1064 nm (Quanta-Ray GCR-170, Spectra-Physics, USA) was used as the IR source with a maximum power output of 50 mW cm^{-2}. The resistance changes of the nc-graphene circuit before and after illumination with an IR laser were monitored using a digital multimeter (TestLink, India) with computer control.

3. Results and discussion

EBICD is a well-known phenomenon where the electron-beam induces the formation of carbonaceous species from residual hydrocarbons abundant in the vacuum chamber. The SEM vacuum chamber used in this study is pumped by an oil-free turbomolecular pump (at a base pressure of 10^{-4} Torr) which is backed by a scroll pump. At this vacuum, the main residual gases are found to be water and oxygen along with a little nitrogen. The hydrocarbon species in the vacuum chamber may also originated from the degassing of the sample holder, conducting glue etc which can cause EBICD

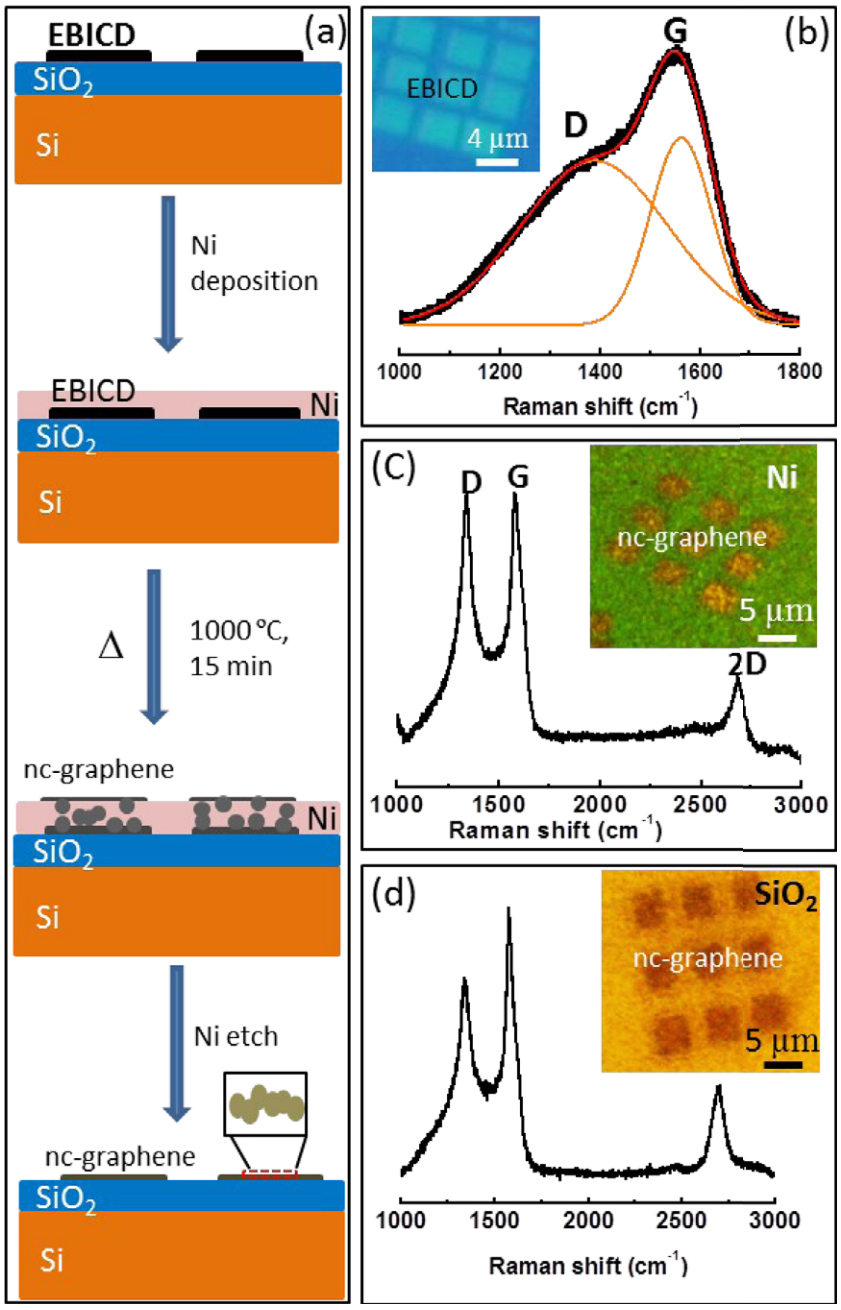

Figure 1. (a) Schematic illustration of the growth of nc-graphene patterns from the EBIC deposits. Each stripe of EBICD is comprised of interconnected nanocrystalline domains of graphene after vacuum annealing in the presence of a Ni layer. Raman spectra of the as deposited EBICD (b), precipitated nc-graphene patterns on the Ni (c) and SiO_2/Si (d). The corresponding optical micrographs of the EBIC deposits, nc-graphene patterns before and after Ni etching are shown in the insets of (b)–(d).

under the intense electron beam. The 'source' is therefore virtually unlimited, thus ensuring the quality of the deposit and prolonged patterning [26]. The hydrocarbon molecules become cross-linked by the electron-beam, leading to the formation of solid polymeric carbonaceous deposits. The process of EBICD is well discussed in the literature [24–29].

The Raman spectrum of the EBIC deposit (~5 nm thick) on SiO_2/Si is shown in figure 1(b). After deconvoluting the spectrum, the D band appears as a shoulder to the G band with the positions of the D and G bands centered around 1392 cm^{-1} (line width, 278 cm^{-1}) and 1559 cm^{-1} (line width, 128 cm^{-1}), respectively (see figure 1(b)). The D and G bands are broad, with the absence of the 2D band at 2700 cm^{-1} (not shown) indicating that the EBIC deposit obtained under given conditions (see inset of figure 1(b) for its optical image) is predominantly amorphous carbon [31, 32]. Upon Ni deposition followed by vacuum annealing at 1000 °C, due to solubility of carbon in Ni [12–15] the carbon atoms can diffuse through the metal and precipitate as nanocrystallites of graphene on the Ni surface (see the schematic in figure 1(a)). Interestingly, the precipitation of graphene occurred only in those regions on the Ni

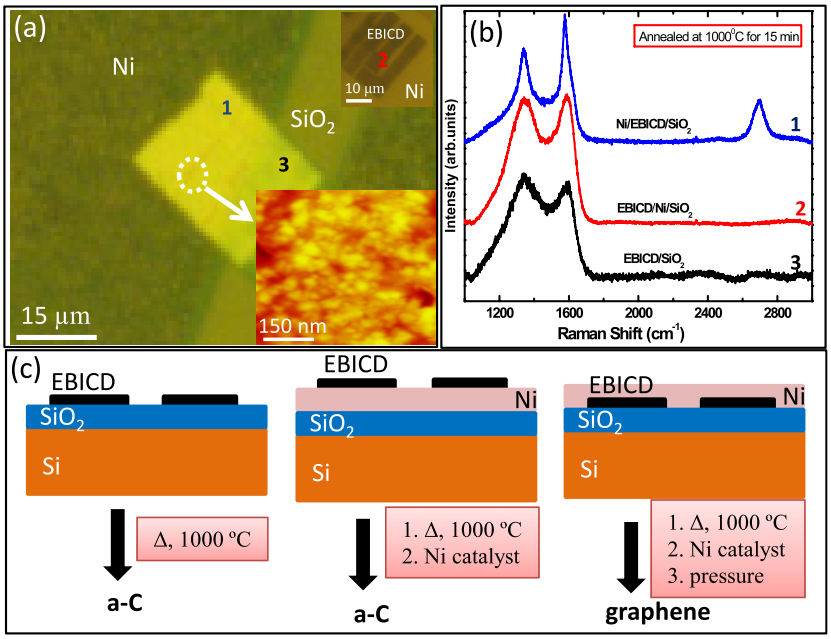

Figure 2. (a) Optical micrograph showing the regions of precipitated nc-graphene on the Ni surface and amorphous carbon (a-C) on the SiO_2 surface after vacuum annealing. The top right inset shows an optical micrograph of the annealed EBIC deposits on the Ni surface. The bottom right inset shows the AFM topography of the nanocrystallites of graphene. (b) Raman spectra of the annealed samples of $EBICD/SiO_2$, $EBICD/Ni/SiO_2$, and $Ni/EBICD/SiO_2$ indicated by curves 3, 2, and 1 respectively. (c) Schematic demonstrating suitable conditions for the growth of graphene from the EBICD layer.

surface where there was a supply of carbon feedstock from the predefined EBICD patterns on the SiO_2 surface (see figure 1(c) and figure S1, supporting information available at stacks.iop.org/Nano/23/425301/mmedia). The Raman spectrum is recorded from the precipitated regions and it is observed that the D (1350 cm^{-1}) and G (1585 cm^{-1}) bands (see schematic in figures 1(a) and (c)) became significantly sharp (line widths of 90 and 40 cm^{-1}, respectively) with the evolution of the 2D band at 2690 cm^{-1}. It is noteworthy that the underlying patterns of nc-graphene remained intact on the SiO_2/Si substrate after etching away the Ni layer in concentrated nitric acid (compare insets in figures 1(c) and (d)). The corresponding Raman spectrum (figure 1(d)) contained a D band with diminished intensity and a 2D band with slightly higher intensity. The I_D/I_G ratio of ~0.6 corresponds to the average crystallite size of 30 nm [31, 32]. The crystallite size (L_a) is calculated using the following formula [32].

$$L_a\ (\text{nm}) = (2.4 \times 10^{-10})\lambda^4 (I_D/I_G)^{-1}$$

where λ is the excitation wavelength.

The control parameters for the growth of nc-graphene such as temperature, time and different thicknesses of Ni have been studied (see figures S2 and S3 in supporting information available at stacks.iop.org/Nano/23/425301/mmedia). The I_D/I_G ratio decreases from 1.2 to 0.2 with increasing annealing temperature from 600 to 1100 °C. The crystallite size also increases accordingly from 5 to 70 nm (see figure S2(b), supporting information available at stacks.iop.org/Nano/23/425301/mmedia). Importantly, the evolution of the 2D band at ~2690 cm^{-1} as a single peak with line width of 70 cm^{-1} (see figure 1(d)) signifies the turbostratic nature of the graphene layers produced by this method [31–33]. The 2D band intensity is somewhat lower due to the presence of intense D band [34, 35], but this is something that is typical of nc-graphene [19, 20]. The Raman spectrum looks similar to that of nc-graphene produced by various other methods in the literature (see table-S1, supporting information available at stacks.iop.org/Nano/23/425301/mmedia). The I_G/I_{2D} ratio is in the range of 2.5–3.5, indicating the presence of regions containing few- to multi-layer graphene [36]. The crystalline nature of the nc-graphene is also evident from the TEM measurements (figure S4 in supporting information available at stacks.iop.org/Nano/23/425301/mmedia).

In order to examine the role of Ni in catalyzing the growth of graphene crystallites, an experiment was carried out where Ni deposition was performed over the EBICD layer in a selective manner using a TEM grid as the shadow mask. The substrate was subjected to thermal treatment at 1000 °C for 15 min under vacuum conditions. This is found optimal as longer durations (>15 min) may lead to the decomposition of SiO_2 under vacuum conditions [12, 13]. The optical micrograph of the thermally treated EBIC layer between two Ni pads is shown in figure 2(a). The AFM topography of precipitated graphene crystallites on the Ni surface (see inset of figure 2(a)) shows nanocrystalline domains of 20–30 nm in width. Raman spectra were recorded from the different regions marked as 1, 2 and 3, as shown in figure 2(b). The 2D band is seen in the spectrum recorded from the $Ni/EBICD/SiO_2$ sample (see spectrum 1) while it is absent in the case of $EBICD/Ni/SiO_2$ (spectrum 2, figure 2(b)) and $EBICD/SiO_2$ samples (spectrum 3, figure 2(b)). Moreover,

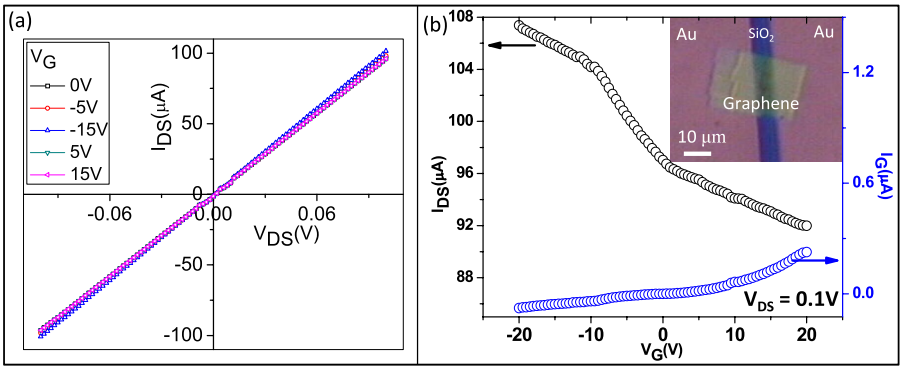

Figure 3. (a) Output and (b) transfer characteristics of the nc-graphene derived from EBICD. The blue curve is for the gate leakage current. The inset shows the nc-graphene between Au source–drain electrodes.

spectra '2' and '3' consist of broad D and G bands, indicating the amorphous nature of carbon. Thus it is evident that the Ni capping layer indeed plays a key role in crystallizing the amorphous carbon in the EBIC deposit into nc-graphene [15]. Based on the above observations, the conditions favorable for the growth of graphene from EBICD can be explained as in the schematic in figure 2(c). EBICD on SiO_2 or on a Ni surface (Ni/SiO_2) followed by vacuum annealing leads to the formation of amorphous carbon (see spectra 3 and 2 of figure 2(b)). In the case of CVD grown graphene, it is customary to have the graphene grown over the metal catalyst [10]. However, this represents a scenario in which there is constant supply of hydrocarbon, in contrast to the present case where the carbon source from EBICD is limited during annealing. When the Ni layer is deposited on top of the EBIC layer, it results in the formation of graphene following thermal treatment. This provides strong evidence that Ni is indeed playing two roles, namely as a capping layer (to build enough pressure and prevent complete volatilization of hydrocarbon species during the heat treatment) and as a catalyst to induce the growth of crystalline sp^2 carbon (see figure S5 available at stacks.iop.org/Nano/23/425301/mmedia).

Transistor characteristics recorded on a device using a nc-graphene strip (24 μm wide) as the active element are shown in figure 3. The AFM topography and the Raman spectrum of the nc-graphene between the Au source–drain contacts are shown in figure S6 in the supporting information (available at stacks.iop.org/Nano/23/425301/mmedia). Temperature dependence conductivity of the nc-graphene showed linear dependence which is typical of a semimetal (see figure S7 in supporting information available at stacks.iop.org/Nano/23/425301/mmedia). The enhanced electrical transport across the nanocrystalline domains of the graphene is clear from its nonexponential $\sigma(T)$ dependence; a similar dependence was also observed for the other semimetallic systems such as nc-graphene obtained from the self-assembled monolayers after annealing at high temperatures [37]. In the output characteristics, the I_{DS} (source–drain current) versus V_{DS} (source–drain voltage) curve is linear, indicating an Ohmic contact between the nc-graphene pattern and the Au electrodes. This linear behavior is akin to graphene and nc-graphene produced by various methods with the absence of saturation in the currents [12–15, 37]. The characteristics show corresponding changes for varying gate voltages (−15, −5, 0, 5 and 15 V; see figure 3(a)). The transfer characteristics (figure 3(b)) reveal a p-type behavior with holes as charge carriers. The carrier (hole) mobility, μ, was estimated from the channel trans-conductance ($g_m = 4.6 \times 10^{-7}$ A V^{-1}) of the FET, $g_m = (dI_{DS}/dV_G) = (W/L)\mu C_0 V_{DS}$ in the linear regime of the I_{DS}–V_G curve, where W/L is the width-to-length ratio of the channel and C_0 is the gate capacitance per unit area [8]. The W/L for the given device is equal to 4. For 300 nm SiO_2, C_0 is about 12 nF cm^{-2}, and based on this value, the hole mobility was derived to be $\mu_h \sim$ 90 cm^2 V^{-1} s^{-1}. The gate leakage curve is shown as blue curve in figure 3(b) which is three orders of magnitude smaller than the channel current. The transfer curves for the same device at different source–drain voltages are shown in the supporting information (figure S8, available at stacks.iop.org/Nano/23/425301/mmedia). The mobility of nc-graphene depends on the size of the graphene crystallites (which can be controlled through annealing temperature) and also the interaction of nc-graphene with the bottom SiO_2 surface [37, 38].

It has been shown that FETs based on large-area single- or few-layer graphene serve as ultrafast photodetectors [39]. Reduced graphene oxide and graphene nanoribbons have been shown to be materials for IR photodetectors [40–42]. The photo-response of our nc-graphene (in the two-probe configuration) towards an IR laser (1064 nm) is shown in figure 4. The change in the current was monitored (figure 4(a)) while turning the IR laser on and off repeatedly five times with a time interval of 60 s. Accordingly, there was an increase and decrease in the current as the laser beam was turned on and off, respectively. The increase in the base current for every cycle is due to thermal effects after illuminating with the IR beam as well as the photoexcitation [40–42]. The photo-response was found to be 23%, calculated after dividing the dark current by the change in the current due to IR illumination [39–42]. The photocurrent increased linearly with increasing laser power (see figure 4(b)). The time constants for the growth and decay of the photocurrent were calculated after fitting with

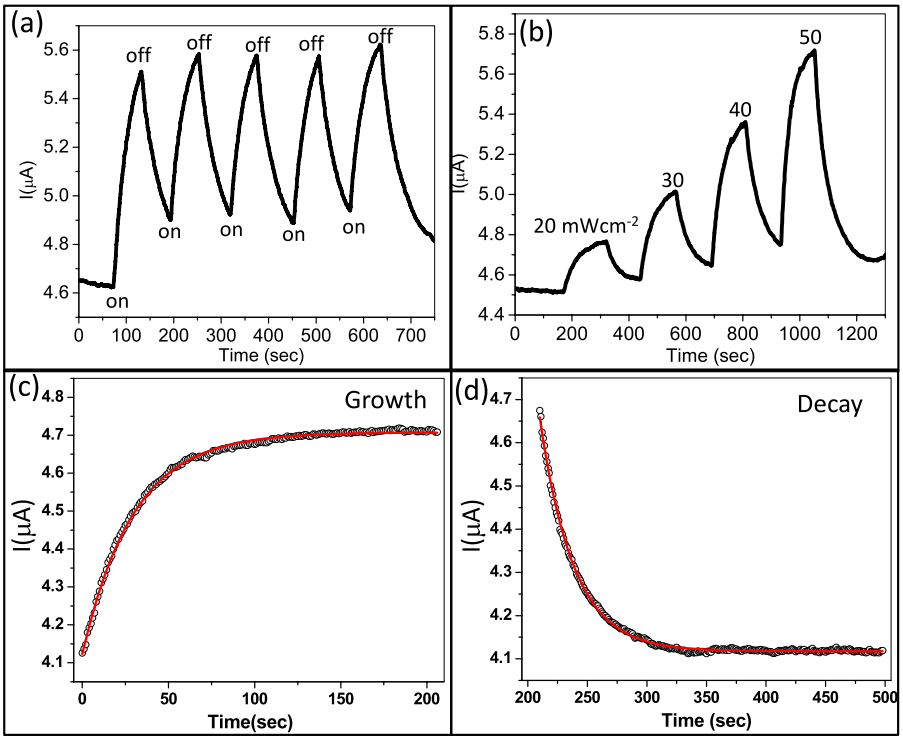

Figure 4. (a) Photo-response curve for five cycles with turning on and off of the IR laser. (b) The photo-response behavior for different laser energies. (c) Growth and (d) decay of the photocurrent of the nc-graphene in response to turning on and off of the IR laser.

the exponential functions (see figures 4(c) and (d)) and they were found to be 28 and 30 s, respectively. The time response is much slower for our nc-graphene than for large area graphene, which is of the order of picoseconds [39]. Another similar device showed a photo-response of 16% (figure S9 in supporting information available at stacks.iop.org/Nano/23/425301/mmedia). The slower response times when compared with the large area graphene devices can be attributed to the presence of disorder and interfaces in the nc-graphene [40]. The scattering of charge carriers by the traps and boundaries can also lead to a slower time response.

It is worth mentioning that our nc-graphene showed a lower mobility ($\sim$90 cm^2 V^{-1} s^{-1}) than the crystalline carbon nanomaterials (carbon nanotubes, graphene and graphene nanoribbons) produced by various synthesis methods (mobilities $>$1000 cm^2 V^{-1} s^{-1}). But mobilities of nc-graphene are much higher than those of amorphous carbon based devices [43]. Moreover, the nc-graphene produced in our method exhibits a higher mobility than the nc-graphene produced by other methods (see table S1 in supporting information available at stacks.iop.org/Nano/23/425301/mmedia). There are other factors such as density of defects in nc-graphene domains and the electronic coupling among the domains as well as with the source–drain electrodes that may have a strong influence on the mobility and photo-response behavior. This demands a separate study.

The novelty of the present study based on EBICD deserves some mention. First, it does not require a hydrocarbon source to be connected and consumed in the process; the source is the 'vacuum' itself. Degassing and residuals in the vacuum can be an ample supply of hydrocarbon. EBICD is a direct way of patterning residual hydrocarbon species into carbonaceous deposits which further can be transformed into graphene patterns with the help of a catalytic Ni layer through thermal treatment. This technique offers to obtain graphene patterns with a smaller number of processing steps over the graphene derived from other solid carbon sources in the literature [12–15]. The EBIC layer can withstand even harsh acid and base environments. On the other hand, most polymers suffer from solubility issues while processing and patterning them on a given substrate. For example, we have also demonstrated the growth of graphene from PMMA through thermal treatment in the presence of a Ni catalyst layer (see figure S10 in supporting information available at stacks.iop.org/Nano/23/425301/mmedia). PMMA requires additional steps for processing and patterning, which is not the case for EBICD, although both processes finally lead to graphene of a similar quality. The other advantage of converting EBIC deposit into graphene is that the thickness of graphene can be well controlled through the initial thickness of the EBIC deposit (which in turn can be controlled through electron dosage conditions). The lateral dimensions of the EBIC deposit can be tuned from the millimeter to the nanometer range using focused and flooded electron beams, respectively. The graphene features of different geometrical shapes can also be realized using this technique. By depositing Ni at specific locations on an EBIC layer, one can have domains of nc-graphene and amorphous carbon in a desired fashion which may have interesting electronic applications. This technique offers transfer-free growth of graphene on insulating surfaces. Though the graphene produced in this method is nanocrystalline in nature, the quality of graphene can be improved by coating a higher thickness (300 nm) of Ni [12–15].

4. Conclusions

Electron beam induced carbonaceous deposits have been transformed into patterns of nanocrystalline (nc) graphene on SiO_2 substrate directly through vacuum annealing using a Ni capping layer. Thus patterned nc-graphene has been effectively employed as an active channel material in FETs. The FET devices exhibit p-type behavior with a mobility of $\sim$90 cm^2 V^{-1} s^{-1}. Nanocrystalline-graphene was found to be sensitive to IR radiation and showed a photo-response of 23%.

Acknowledgments

The authors thank Professor C N R Rao, FRS for his encouragement. Support from the Department of Science and Technology, Government of India is gratefully acknowledged. NK and VSB acknowledge CSIR for funding. NK thanks Dr Abhay for FET measurements and Ms Kiruthica for help with the temperature dependant electrical measurements. GUK acknowledges the Sheikh Saqr Senior Fellowship. The authors thank the Veeco India Nanotechnology Laboratory at the Jawaharlal Nehru Centre for Advanced Scientific Research for the AFM facility.

References

[1] Robertson J 1991 Hard amorphous (diamond-like) carbons *Prog. Solid State Chem.* **21** 199
[2] Robertson J 1994 Diamond-like carbon *Pure Appl. Chem.* **66** 1789
[3] Dresselhaus M S, Dresselhaus G and Eklund P C 1996 *Science of Fullerenes and Carbon Nanotubes* (NewYork: Academic)
[4] Geim A K and Novoselov K S 2007 The rise of graphene *Nature Mater.* **6** 183
[5] Wei D and Liu Y 2010 Controllable synthesis of graphene and its applications *Adv. Mater.* **22** 3225
[6] Novoselov K S, Geim A K, Morozov S V, Jiang D, Zhang Y, Dubonos S V, Grigorieva I V and Firsov A A 2004 Electric field effect in atomically thin carbon films *Science* **306** 666
[7] Li X L, Wang X R, Zhang L, Lee S W and Dai H J 2008 Chemically derived, ultrasmooth graphene nanoribbon semiconductors *Science* **319** 1229
[8] Tang Y B *et al* 2009 High-quality graphenes via a facile quenching method for field-effect transistors *Nano Lett.* **9** 1374
[9] Hernandez Y *et al* 2008 High-yield production of graphene by liquid-phase exfoliation of graphite *Nature Nanotechnol.* **3** 563
[10] Di C A, Wei D C, Yu G, Liu Y Q, Guo Y L and Zhu D B 2008 Patterned graphene as source/drain electrodes for bottom-contact organic field-effect transistors *Adv. Mater.* **20** 3289
[11] Ruan G, Sun Z, Peng Z and Tour J M 2011 Growth of graphene from food, insects, and waste *ACS Nano* **5** 7601
[12] Yan Z, Peng Z, Sun Z, Yao J, Zhu Y, Liu Z, Ajayan P M and Tour J M 2011 Growth of bilayer graphene on insulating substrates *ACS Nano* **5** 8187
[13] Peng Z, Yan Z, Sun Z and Tour J M 2011 Direct growth of bilayer graphene on SiO_2 substrates by carbon diffusion through nickel *ACS Nano* **5** 8241
[14] Shin H-J *et al* 2011 Transfer-free growth of few-layer graphene by self-assembled monolayers *Adv. Mater.* **23** 4392
[15] Byun S-J, Lim H, Shin G-Y, Han T-H, Oh S H, Ahn J-H, Choi H C and Lee T-W J 2011 Graphenes converted from polymers *Phys. Chem. Lett.* **2** 493
[16] Zheng M *et al* 2010 Metal-catalyzed crystallization of amorphous carbon to graphene *Appl. Phys. Lett.* **96** 063110
[17] Orofeo C M, Ago H, Hu B and Tsuji M 2011 Synthesis of large area, homogeneous, single layer graphene films by annealing amorphous carbon on Co and Ni *Nano Res.* **4** 531
[18] Hatakeyama T, Kometani R, Warisawa S and Ishihara S 2011 Selective graphene growth from DLC thin film patterned by focused-ion-beam chemical vapor deposition *J. Vac. Sci. Technol.* B **29** 06FG04
[19] Sun J, Lindvall N, Cole M T, Wang T, Booth T J, Bøggild P, Teo J, Liu K B K and Yurgens A 2012 Controllable chemical vapor deposition of large area uniform nanocrystalline graphene directly on silicon dioxide *J. Appl. Phys.* **111** 044103
[20] Lee C M and Choi J 2011 Direct growth of nanographene on glass and postdeposition size control *Appl. Phys. Lett.* **98** 183106
[21] Kalita G, Kayastha M S, Uchida H, Wakita K and Umeno M 2012 Directgrowth of nanographene films by surface wave plasma chemical vapordeposition and their application in photovoltaic devices *RSC Adv.* **2** 3225
[22] Zhang L, Shi Z, Wang Y, Yang R, Shi D and Zhang G 2011 Catalyst-freegrowth of nanographene films on various substrates *Nano Res.* **4** 315
[23] Kurra N, Sagade A A and Kulkarni G U 2011 Ultrafast direct ablative patterning of HOPG by single laser pulses to produce graphene ribbons *Adv. Funct. Mater.* **21** 3836
[24] Miura N, Ishii H, Shirakashi J, Yamada A and Konagai M 1997 Electron-beam-induced deposition of carbonaceous microstructures using scanning electron microscopy *Appl. Surf. Sci.* **113/114** 269
[25] Ding W, Dikin D A, Chen X, Piner R D, Ruoff R S, Zussman E, Wang X and Li X 2005 Mechanics of hydrogenated amorphous carbon deposits from electron-beam-induced deposition of a paraffin precursor *J. Appl. Phys.* **98** 014905
[26] Kurra N, Kumar T V and Kulkarni G U 2011 CNT manipulation: inserting a carbonaceous dielectric layer beneath using electron beam induced deposition *J. Nanosci. Nanotechnol.* **11** 1025
[27] Morita N, Kawasegi N and Ooi K 2008 Three-dimensional fabrication on GaAs surfaces using electron-beam-induced carbon deposition followed by wetchemical etching *Nanotechnology* **19** 155302
[28] Rice P, Wallis T M, Russek S E and Kabos P 2007 Broadband electrical characterization of multiwalled carbon nanotubes and contacts *Nano Lett.* **7** 1086
[29] Yu M-F, Lourie O, Dyer M J, Moloni K, Kelly T F and Ruoff R S 2000 Strength and breaking mechanism of multiwalled carbon nanotubes under tensile load *Science* **287** 637
[30] Pavan Kumar G V and Narayana C 2007 Adapting a fluorescence microscope to perform surface enhanced Raman spectroscopy *Curr. Sci.* **93** 778
[31] Ferrari A C and Robertson J 2000 Interpretation of Raman spectra of disordered and amorphous carbon *Phys. Rev.* B **61** 14095
[32] Pimenta M A, Dresselhaus G, Dresselhaus M S, Cançado L G, Jorioa A and Saito R 2007 Studying disorder in graphite-based systems by Raman spectroscopy *Phys. Chem. Chem. Phys.* **9** 1276
[33] Malard L M, Pimenta M A, Dresselhaus G and Dresselhaus M S 2009 Raman spectroscopy in graphene *Phys. Rep.* **473** 51
[34] Cançado L G, Jorio A, Ferreira E H M, Stavale F, Achete C A, Capaz R B, Moutinho M V O, Lombardo A, Kulmala T S and Ferrari A C 2011 Quantifying defects in graphene via Raman spectroscopy at different excitation energies *Nano Lett.* **11** 3190
[35] Jorio A, Lucchese M M, Stavale F, Ferreira E H M, Moutinho M V O, Capaz R B and Achete C A 2010 Raman

study of ion-induced defects in *N*-layer graphene *J. Phys.: Condens. Matter* **22** 334204
[36] Ferrari A C *et al* 2006 Raman spectrum of graphene and graphene layers *Phys. Rev. Lett.* **97** 187401
[37] Turchanin A, Weber D, Büenfeld M, Kisielowski C, Fistul M V, Efetov K B, Weimann T, Stosch R, Mayer J and Gölzhäuser A 2011 Conversion of self-assembled monolayers into nanocrystalline graphene: structure and electric transport *Acs Nano* **5** 3896
[38] Bolotin K I, Sikes K J, Hone J, Stormer H L and Kim P 2008 Temperature-dependent transport in suspended graphene *Phys. Rev. Lett.* **101** 096802
[39] Xia F, Mueller T, Lin Y-M, Valdes-Garcia A and Avouris P 2009 Ultrafast graphene photodetector *Nature Nanotechnol.* **4** 839
[40] Ghosh S, Sarker B K, Chunder A, Zhai L and Khondaker S I 2010 Position dependent photodetector from large area reduced graphene oxide thin films *Appl. Phys. Lett.* **96** 163109
[41] Chitara B, Panchakarla L S, Krupanidhi S B and Rao C N R 2011 Infrared photodetectors based on reduced graphene oxide and graphene nanoribbons *Adv. Mater.* **23** 5419
[42] Ryzhii V, Mitin V, Ryzhii M, Ryabova N and Otsuji T 2008 Device model for graphene nanoribbon phototransistor *Appl. Phys. Exp.* **1** 063002
[43] Kurra N, Bhadram V S, Narayana C and Kulkarni G U 2012 Field-effect transistors based on thermally treated electron beam-induced carbonaceous patterns *ACS Appl. Mater. Interfaces* **4** 1030